

# Properties of self gravitating quasi-stationary states

Francesco Sylos Labini<sup>1,2,3</sup> and Roberto Capuzzo-Dolcetta<sup>4,1</sup>

<sup>1</sup> CREF, Centro Ricerche Enrico Fermi, Via Panisperna 89A, I-00184, Roma, Italy

<sup>2</sup> Istituto dei Sistemi Complessi, Consiglio Nazionale delle Ricerche, I-00185 Roma, Italy

<sup>3</sup> Istituto Nazionale Fisica Nucleare, Dipartimento di Fisica, Università “Sapienza”, I-00185 Roma, Italy

<sup>4</sup> Dipartimento di Fisica, Sapienza, Università di Roma, piazzale Aldo Moro 2, I-00185, Roma, Italy

Received / Accepted

**Abstract.** Initially far out-of-equilibrium self-gravitating systems form, through a collisionless relaxation dynamics, quasi-stationary states (QSS). These may arise from a bottom-up aggregation of structures or in a top-down frame; their quasi-equilibrium properties are well described by the Jeans equation and are not universal, i.e. they depend on initial conditions. To understand the origin of such dependence, we present results of numerical experiments of initially cold and spherical systems characterized by various choices of the spectrum of initial density fluctuations. The amplitude of such fluctuations determines whether the system relaxes in a top-down or a bottom-up manner. We find that statistical properties of the resulting QSS mainly depend upon the amount of energy exchanged during the formation process. In particular, in the violent top-down collapses the energy exchange is large and the QSS show an inner *core* with an almost flat density profile and a quasi Maxwell-Boltzmann (isotropic) velocity distribution, while their outer regions display a density profile  $\rho(r) \propto r^{-\alpha}$  ( $\alpha > 0$ ) with radially elongated orbits. We analytically show that  $\alpha = 4$  in agreement with numerical experiments. In the less violent bottom-up dynamics, the energy exchange is much smaller, the orbits are less elongated and  $0 < \alpha(r) \leq 4$ , with a density profile well fitted by the Navarro-Frenk-White behavior. Such a dynamical evolution is shown by both non-uniform spherical isolated systems and by halos extracted from cosmological simulations. We consider the relation of these results with the *core-cusp* problem concluding that this is naturally solved if galaxies form through a monolithic collapse.

**Key words.** Methods: numerical; Galaxies: formation; Galaxies: halos.

## 1. Introduction

Unlike typical short-range interacting systems, which tend to relax to thermodynamical equilibria through collisions, long-range interacting ones are driven to quasi-equilibrium configurations (or quasi-stationary states — QSS) by a mean-field collisionless relaxation dynamics. These QSS are close to virial equilibrium and their lifetime diverges with the number of particles  $N$  because of the decreasing effect of two-body encounters (Lynden-Bell 1967; Padmanabhan 1990; Dauxois et al. 2002; Campa et al. 2014; Levin et al. 2014; Capuzzo-Dolcetta 2019). A comprehension of the statistical properties of the QSS requires the understanding of how their dynamics determines the evolution of the system from an out-of-equilibrium condition to a quasi-stationary configuration.

If the long-range force at work is self-gravity, QSS are reached in two different frames, corresponding respectively to that of a finite and isolated system or to that of a system ‘embedded’ in an expanding space, this latter representing

a typical cosmological case. In both cases, depending on the initial conditions (IC), the dynamics may correspond to a *top-down* monolithic collapse or to a *bottom-up* aggregation of substructures. In this work we will single out the properties of the IC determining which evolutionary path brings a certain configuration towards a QSS, regardless the system is finite and isolated or embedded in an infinite expanding background.

The top-down monolithic collapse is modeled, in the simplest way, as the progression of a gravitational instability out of the linearity, as it happens when the overdensity is such that the selfgravity dominates over the expanding background (Peebles 1980). Actually, if the amplitude of a local overdensity is large enough then tidal effects of neighboring density perturbations can be neglected and its evolution proceeds, essentially, as that of an isolated perturbation: these are precisely the hypotheses assumed in the paradigmatic, non-linear, gravitational instability model that is analytically solvable, i.e. the spherical collapse model (Sahni & Coles 1995). Indeed, the evolution of an isolated overdensity in an expanding background should reproduce, in

physical coordinates, that obtained in open boundary conditions without expansion (Joyce & Sylos Labini 2013). The collapse and stabilization of such an over-density has been studied since the first numerical experiments with self-gravitating systems, in both isolated and embedded cases (Henon 1964; van Albada 1982; Aarseth et al. 1988; Aguilar & Merritt 1990; Theis & Spurzem 1999; Boily et al. 2002; Roy & Perez 2004; Boily & Athanassoula 2006; Barnes et al. 2009; Joyce et al. 2009; Sylos Labini 2012; Worrakitpoonpon 2015; Merritt & Aguilar 1985; Aguilar & Merritt 1990; Theis & Spurzem 1999; Sylos Labini 2013b; Sylos Labini et al. 2015; Benhaïem & Sylos Labini 2015; Benhaïem et al. 2016; Benhaïem & Sylos Labini 2017; Spera & Capuzzo-Dolcetta 2017).

On the other hand, a QSS can be originated from a bottom-up hierarchical aggregation process, in which smaller substructures merge to form larger and larger ones. If the system is infinite this process continues without ending while if the system is finite the aggregation eventually halts. Bottom-up structure formation is typical of standard cosmological scenarios, like the cold dark matter (CDM) one, because of the long-range nature of density correlations (Blumenthal et al. 1982; Bond et al. 1982; Peebles 1980; Blumenthal et al. 1984). In the case of cosmological systems, if the velocity dispersion is large then the collapse occurs for objects that are big enough to make their gravitational potential overcoming the ‘pressure’ due to random motions, that corresponds to the so-called hot dark matter scenarios. In this latter case, density correlations have a sharp cut-off beyond a scale which corresponds to the size of the perturbations that first become nonlinear (Peebles 1980).

The statistical properties of the QSS depend on which of the two evolutionary paths described above was actually followed by the system in exam. In particular, we will show in this paper that these properties are essentially related to the violence, in terms of the particle energy variation, of the process leading toward settling the system in a QSS: this being very quick in the case of a top-down monolithic collapse while slower for a hierarchical, bottom-up, aggregation process.

The focus of our study is the investigation of QSS with power-law density profiles and for this reason we consider cold IC that correspond to far out-of-equilibrium configurations, i.e., with a virial ratio<sup>1</sup>  $|Q| \ll 1$ : if  $|Q| \approx 1$  then the collapse is inhibited and the system relaxes gently to form a compact core with a exponentially decaying density profile (Sylos Labini 2013b; Benetti et al. 2014).

In order to study the two dynamical mechanisms outlined above, in this paper we consider, through numerical  $N$ -body experiments, the evolution of simple systems corresponding to finite spherical distributions with different initial density fluctuations power spectra. Changing the amplitude of such fluctuations allows to pass from a

top-down to a bottom-up process, and thus to explore the full dynamics phase-space. This study aims to develop a unified understanding of the properties of the QSS generated by both dynamical mechanisms. Then, we also consider the properties of QSS formed in cosmological  $N$ -body simulations, i.e., the so-called halos. To this purpose we consider halos extracted from the Abacus simulations (Garrison et al. 2018, 2019) where a CDM scenario has been adopted. We show that their properties can be understood in the same theoretical framework developed above discussing the reason for such a case.

The paper is organized as follows. In Sect.2 we present the main characteristics of our  $N$ -body experiments for isolated systems we have considered and of those of the the Abacus simulations leading to cosmological halos. In Sect.3 we discuss the case of models of uniform and non-uniform spherical collapses that show the transition from a bottom-up to a top-down clustering. The properties of cosmological halos are also considered. The astrophysical implications of our findings are discussed in Sect.4 where we also draw our conclusions.

## 2. Models and methods

### 2.1. Isolated systems

We have considered two types of IC in our numerical experiments of finite systems. The first is represented by spherical, isolated, spatially homogeneous and cold overdensities of  $N$  particles of mass  $m$  with zero initial velocity in which particles are randomly distributed, i.e. have Poisson density fluctuations

$$\delta = \sqrt{\frac{\langle \Delta N^2 \rangle}{\langle N \rangle^2}} \sim N^{-1/2}.$$

In order to explore the role of fluctuations we have let  $N$  vary in the range  $10^4 - 10^6$  while the total mass and size of the system are taken constant. We have chosen a normalization to an astrophysical object; the total mass is  $M = 10^{10} M_\odot$ , the initial radius is  $R_0 = 100$  kpc so that the free-fall time

$$\tau_{ff} \approx \frac{1}{\sqrt{G\rho}} \approx 1.5 \text{ Gyr} \quad (1)$$

where  $\rho = 3M/(4\pi R_0^3)$  is the system density. As mentioned in the introduction, the most violent evolution occurs, of course, when the initial velocity dispersion is zero ( $Q = 0$ ); when the initial virial ratio is in the range  $-0.5 < Q < 0$  then the collapse is less violent but, qualitatively, the dynamical evolution remains the similar to that of  $Q = 0$  (Sylos Labini 2013b). For warmer IC, i.e.  $-1 < Q < -0.5$ , instead, when the collapse is halted by the effect of the large velocity dispersion and the system reaches a configuration characterized by a compact core a very diluted halo (Benetti et al. 2014). We focus the attention on cold IC because only for that case a non-trivial power-law density profile is found to develop.

<sup>1</sup> the virial ratio  $q$  is here defined as  $Q \equiv \frac{2K}{W}$ , where  $K$  and  $W$  are, respectively, the total kinetic and potential energy.

The second family of IC is still represented by isolated, almost spherical, spatially homogeneous and cold systems that have the same  $M, R_0$  as before, but having initial density fluctuations larger than Poisson ones. These are generated by randomly distributing  $N_c$  points in a sphere of radius  $R$ . Each of these points is then considered as a center of a spherical sub-system of  $N_p$  particles that are also randomly distributed in a smaller spherical volume. We take the radius of each subsystem to be  $r_s = 2\Lambda_c$  where  $\Lambda_c$  is the average distance between the  $N_c$  particles, i.e.  $\Lambda_c = 0.55(3N_c/3\pi R_0^3)^{1/3}$ . In this way a moderate overlap between different sub-clumps is allowed so too smooth out initial fluctuations when  $N_c$  is sufficiently large, i.e.  $N_c > 10^2$ . The total number of particles is thus  $N = N_c \times N_p \approx 10^6$ . A realization can be characterized by the parameter

$$\gamma = \frac{N}{N_c} \quad (2)$$

where we have chosen  $\gamma \in [10, 10^5]$  where  $\gamma = 10^5$  for the initially strongly clustered case and  $\gamma = 10$  for the less clustered one. Indeed, the smaller is  $N_c$ , the larger is  $\gamma$  and the larger are the initial fluctuations  $\delta \sim N_c^{-1/2} \sim (\gamma/N)^{1/2}$  in sufficiently large scale  $r > \Lambda_c$ . The initial velocities are taken to be zero as in the previous case.

## 2.2. The code

All our simulations have been performed by means of the publicly available and widely used code **Gadget-2** (Springel 2005). The gravitational interaction is evaluated by direct summation over close neighbors and via a multi-polar expansion on a larger scale. In this way, the number of computations is sensibly lower compared to the usual  $N^2$  scaling, characteristic of the direct-summation  $N$ -body algorithms. The gravitational interaction on the small distance scale is regularized with the so-called gravitational softening  $\varepsilon$ : the force has its purely Newtonian value at separations greater than  $\varepsilon$  ( $r \geq \varepsilon$ ) while it is smoothed at shorter separations. The assumed functional form of the regularized potential, is a cubic spline interpolating between the exact Newtonian potential at  $r = \varepsilon$  and a constant value at  $r = 0$  where the mutual gravitational force vanishes (the exact expression can be found in Springel (2005)). A detailed study of the parameter space of the code **Gadget-2**, for simulations considering only Newtonian gravity, has been reported in Joyce et al. (2009); Sylos Labini (2013b). In the simulations that we discuss in what follows we always keep energy, momentum and angular momentum conservation at a level of precision better than 1%.

The criterion for our choice of softening length  $\varepsilon$  is that this is sufficiently small so the numerical results are independent of it, and we interpret our results as being representative of the limit  $\varepsilon = 0$ . A convergence study by varying  $\varepsilon$  is presented in Joyce et al. (2009) where it was concluded that results are  $\varepsilon$  independent as long the minimal radius of the system  $R_{min}$  during the collapse is larger than  $\varepsilon$ . We take  $\varepsilon = 0.05$  kpc but we have also

considered experiments with  $\varepsilon = 0.005$  kpc. Given that collisional effects are negligible, occurring on much longer time scales than the collapse characteristic time scale, this result can be understood as due to the fact that the system mean-field, whose variation is the source of the dynamics, remains Newtonian as long as  $R_{min} \gg \varepsilon$ .

## 2.3. Cosmological halos

We have analyzed several halo catalogs<sup>2</sup> from the Abacus project (Garrison et al. 2018, 2019). A high resolution simulation was run to produce halos with a relatively large number of particles (i.e.  $N \sim 10^5 - 10^6$ ): this has a total of  $700^3$  particle in a box of side  $L = 200$  Mpc/h. The cosmology was a CDM with a cosmological constant and neutrinos included in the background expansion. With these parameters the particle mass is  $M = 2 \times 10^9 M_\odot$ . Halos are identified by means of the Abacus halo finder, called the CompaSO Halo Finder<sup>3</sup>.

The softening length is fixed in proper, i.e. not comoving, coordinates, and it is chosen to be  $\varepsilon = 7$  kpc/h<sup>4</sup> (Plummer-equivalent, although spline softening was used). Then halo catalogs were generated at a few epochs.

It should be emphasized that there is a long-standing discussion in the literature concerning small scale resolution effects in cosmological  $N$ -body which is still not clarified. Beyond issues of numerical convergence, it is important to understand the limits imposed on the accuracy of results by the use of a finite number of particles to represent the theoretical continuum density field, and the associated introduction of a smoothing scale  $\varepsilon$  in the gravitational force that imposes a lower limit on the spatial resolution. The question of the suitable value of the ratio  $\varepsilon/\ell$  (where  $\ell$  is the initial inter-particle distance) has been the subject of long-standing controversy (see, e.g., Joyce & Sylos Labini (2013); Sylos Labini (2013a); Baushev & Barkov (2018) and references therein). The use of a softening length that is fixed in physical coordinates rather than in comoving coordinates should mitigate the resolution effects but a more detailed study is needed to proof that this is the case. Hereafter we are not going to discuss this issue: rather the point of view we adopt in this work is to study which are the physical properties of the QSS without investigating the difficult problem of whether resolution effects, especially on small scales, has modified them with respect to the ones expected in the proper continuum limit.

<sup>2</sup> Data are available from

<https://lgarrison.github.io/AbacusCosmos/>

<sup>3</sup> This is a hybrid algorithm described in

<https://abacussummit.readthedocs.io/en/latest/compaso.html>

<sup>4</sup> The convention that  $a = 1$  at  $z = 0$  was used, so the proper and comoving softening lengths are both equal to 7 kpc/h at  $z = 0$ .

### 3. Properties of the Quasi Stationary States

#### 3.1. Statistical estimators

Let us call  $k_i$ ,  $\phi_i$  and  $e_i$  the kinetic, potential and total (i.e.,  $e_i = k_i + \phi_i$ ) energy of the  $i$ th particle of the system of fixed mass  $m_i = m$ . Let  $K$ ,  $W$  and  $E = K + W$  the system kinetic, potential and total mechanical energy, and  $M = Nm$  the total system mass. In absence of dissipative mechanisms, the system total energy  $E(t)$  is clearly conserved along the system evolution as well as its total linear and angular momenta. Actually, as mentioned above, by monitoring the behavior of these quantities we have a global control of the accuracy of the numerical integration.

The quantity

$$\Delta(t) = \frac{1}{\langle e(0) \rangle} \sqrt{\frac{\sum_{i=1}^N (e_i(t) - e_i(0))^2}{N}} \quad (3)$$

is a measure of the global exchange of the particle energies over the interval from zero and a generic time  $t$ , in units of the initial average energy per particle

$$\langle e(0) \rangle = \frac{1}{N} \sum_{i=1}^N e_i(t=0). \quad (4)$$

We can consider the estimators

$$\overline{n(\mathbf{r}, t)} = \frac{1}{\Delta V} \sum_{i=1}^{\Delta N(r)} \delta(\mathbf{r} - \mathbf{r}_i, t), \quad (5)$$

$$\overline{k(\mathbf{r}, t)} = \frac{1}{\Delta N} \sum_{i=1}^{\Delta N} k_i(\mathbf{r}, t), \quad (6)$$

$$\overline{\phi(\mathbf{r}, t)} = \frac{1}{\Delta N} \sum_{i=1}^{\Delta N} \phi_i(\mathbf{r}, t), \quad (7)$$

that are volume averages in a sampling volume  $\Delta V$  containing  $\Delta N$  particles of the number density profile (in Eq.5  $\delta(\mathbf{r} - \mathbf{r}_i)$  is the Dirac's delta function), and of the kinetic and potential energy. Other useful statistical indicators are the particle energy distribution,  $p(e)$ , and the velocity distribution  $f(\mathbf{v})$ .

The description of the QSS arising from a non-collisional dynamics can be approached in terms of the self-consistent Vlasov-Poisson system of equations (Binney & Tremaine 2008). When the long-range force is gravity and specified to stellar dynamics, the Vlasov equation turns in the Jeans equation (Jeans 1915; Binney & Tremaine 2008). In spherical symmetry, the Jeans equilibrium implies that the function

$$\psi(r) = - \frac{\frac{\langle v_r^2(r) \rangle}{\rho(r)} \frac{d\rho(r)}{dr} + \frac{d\langle v_r^2(r) \rangle}{dr} + \frac{2\beta(r)\langle v_r^2(r) \rangle}{r}}{\frac{d\phi(r)}{dr}} \approx 1 \quad (8)$$

where, in Eq. 8,  $\rho(r)$  is the mass density,  $v_r(r)/v_t(r)$  the radial/tangential velocity and

$$\beta(r) = 1 - \frac{\langle v_t(r)^2 \rangle}{2\langle v_r(r)^2 \rangle}$$

the anisotropy parameter such that  $\beta = 0$  for isotropic orbits and  $\beta = 1$  for radial orbits.

#### 3.2. Power-law profiles of quasi stationary states

Numerical simulations show that the QSS formed by the collapse of an isolated, cold and initially uniform spherical over-density has a density profile of the type (van Albada 1982; Aarseth et al. 1988; Joyce et al. 2009; Sylos Labini 2012)

$$n_{vr}(r) = \frac{n_0}{1 + \left(\frac{r}{r_0}\right)^4}, \quad (9)$$

where  $n_0, r_0$  are two parameters which depend on the specific case under study.

On the other hand, in the context of cosmological simulations in the CDM scenario, a universal density profile nicely fits the dark matter structures in the highly non-linear regime, the so-called halos. This fitting formula is the so-called NFW profile (Navarro et al. 1997; Taylor & Navarro 2001; Navarro et al. 2004)

$$n(r) = \frac{n_0}{\left(\frac{r}{r_0}\right) \left(1 + \frac{r}{r_0}\right)^2}. \quad (10)$$

The main difference of the profile in Eq.10 stands in its cuspy behaviour and in its shallower decay at large distances ( $r \gg r_0$ ).

It should be noticed that the dynamical processes underlining the formation of the profiles in Eq.9 and Eq.10 are different. Indeed, in CDM models, the clustering proceeds bottom-up through the subsequent merger of structures into larger ones. This happens because initial density fluctuation field are characterized by long-range correlations: indeed, the correlation function decays as  $\sim r^{-1}$  in the range of scales relevant for cosmological structure formation, and, correspondingly, the power spectrum grows as  $\sim k^2$  (where  $k = 2\pi/r$ ) (Peebles 1980). Although halos are commonly considered as the building blocks of non-linear structures formed in a cosmological context, a full theoretical understanding of their properties is still lacking (see, e.g., Theis & Spurzem (1999); Binney & Knebe (2001); Diemand et al. (2004); Levin et al. (2008)).

With regard to the density profile in Eq.9, reached as QSS of an isolated monolithic collapse, it is seen that at virialization, the orbital distribution is radially biased, thing that implies a *non-isotropic* velocity distribution (Sylos Labini 2013b). In what follows we will derive a similar conclusion by using the Jeans equation; further we will show that this analysis can shed light on the more general case of the density profile in Eq.10 that is not characterized by a single exponent.



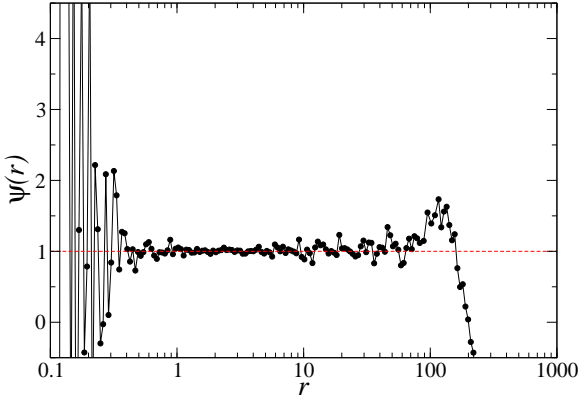


**Fig. 1.** Behavior of the function  $\psi(r)$  defined in Eq.8 at  $t = 9$  Gyr in the case of the initially uniform sphere, with  $N = 10^6$ . At small distances the deviation from  $\psi = 1$  is due to sparse sampling fluctuations while at large distances, (i.e.  $r > 100$  kpc) the deviation is due to the out-of-equilibrium nature of the system.

While upon the assumption of velocity isotropy many solutions for the distribution function (DF) of given spherically symmetric density laws are found, like for example the family of the so called  $\gamma$ -models (Dehnen 1993; Arca-Sedda & Capuzzo-Dolcetta 2014) the correct modeling of *non-isotropic* (in velocity space) systems, like the ones actually coming from both isolated (Sylos Labini 2013b) and non-isolated (Hansen & Moore 2006)  $N$ -body experiments remains an open problem.

### 3.3. The case of a uniform and isolated spherical overdensity

The collapse of an *initially uniform* sphere is a paradigmatic case investigated numerically by a large number of authors (Henon 1964; van Albada 1982; Aarseth et al. 1988; Aguilar & Merritt 1990; Theis & Spurzem 1999; Boily et al. 2002; Roy & Perez 2004; Boily & Athanassoula 2006; Barnes et al. 2009; Joyce et al. 2009; Sylos Labini 2012; Worrakitpoonpon 2015; Merritt & Aguilar 1985; Aguilar & Merritt 1990; Theis & Spurzem 1999; Sylos Labini 2013b; Sylos Labini et al. 2015). The specific key-role played by density fluctuations during the collapse has been studied by, e.g. Aarseth et al. (1988) and Spera & Capuzzo-Dolcetta (2017), while the mechanism of the particle energy change was firstly discussed by Joyce et al. (2009). We are now going to consider the properties of the QSS, that is formed after the virialization, in particular the differentiation between ‘core’ and ‘halo’<sup>5</sup>.

The QSS is in equilibrium and indeed Eq.8 is satisfied (see Fig.1): at small distances the signal is noisy because the number of particles in shells is small, i.e.  $N < 10^2$ , and

<sup>5</sup> Unless specified all distances are expressed in kpc and all times in Gyr. The velocities is measured in km/s.

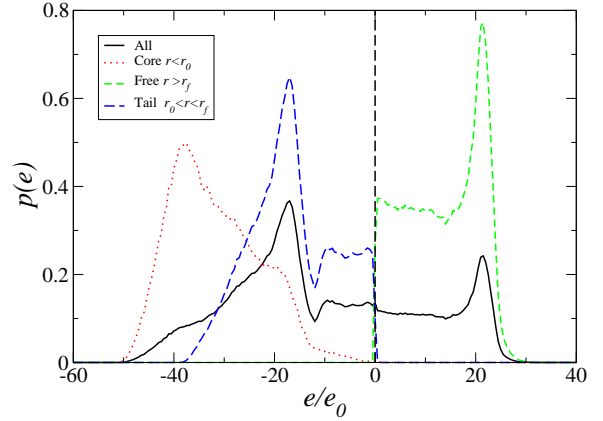


**Fig. 2.** Particle energy distribution of the QSS at  $t = 9$  Gyr in units of  $e_0$  (see Eq.4). The system after the collapse is made of three components: two form the QSS (tail and core) and one, with  $e > 0$ , is made of “free” particles. The core is made of particles having radial distance  $r < r_0$ ; the free particles have positive energy or  $r > r_f$ , where  $r_f = r_f(t)$  must be estimated from the numerical data.

at larger distances, i.e.  $r > 100$  kpc, there is a clear deviation due to the fact that particles have positive energy. The behavior of  $\psi(r)$  for this system represents a useful reference for the analysis of the more complex situations presented in what follows.

#### 3.3.1. The core and the halo

Let us now consider the core and the halo of the QSS separately. The core is defined as the region within the length scale  $r_0$  found by fitting the density profile with Eq.9. Figure 2 shows the normalized particle energy distribution of the QSS at  $t = 9$  Gyr (i.e. at a time much longer than  $\tau_{ff} \approx 1.5$  Gyr); in particular, the three main components of the system after the collapse are highlighted: two of them constitute the actual QSS, namely the core (i.e.,  $r < r_0$ ) and the outermost bound particles that forms the halo ( $r > r_0$  and  $e < 0$ ) while the remaining component is made of free particles.

A gas under steady state conditions at a temperature  $T$  immersed in a conservative force field, is characterized by a distribution function that differs from the Maxwell-Boltzmann (MB) distribution by the exponential factor  $\exp(-\Phi(\mathbf{r})/kT)$ , where in this case the “temperature” can be defined through the particle velocity dispersion. In this situation that the equilibrium distribution function for this case is

$$f(\mathbf{v}, \mathbf{r}) = n_0 \left( \frac{m}{2\pi kT} \right)^{3/2} \exp \left( -\frac{mv^2/2 + \Phi(\mathbf{r})}{kT} \right). \quad (11)$$

Consequently, the number density for a system described by this distribution function is given by

$$n(\mathbf{r}) = n_0 \exp(-\Phi(\mathbf{r})/kT). \quad (12)$$

The velocity distribution function in the core (see the upper and middle panels of Fig.3) is well approximated by

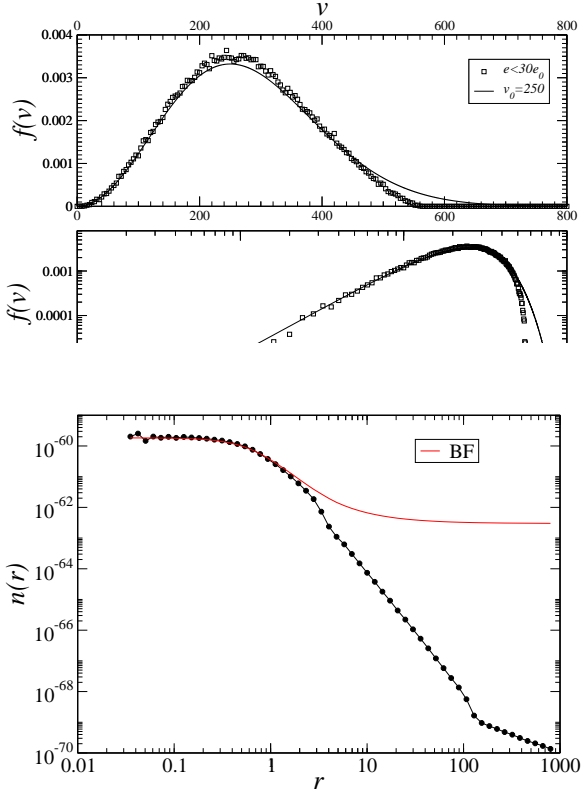


**Fig. 3.** Upper panel: the velocity distribution function in the core by applying a selection i in energy and the corresponding best fit with a MB distribution with  $v_0 = 250$  km/s in linear and (middle panel) bi-logarithmic scale. Bottom panel: measured density profile together with the Boltzmann factor (see Eq.12).

a MB distribution. The fit has been done by defining the core in two different ways: i) all particles with  $r < r_0$  where  $r_0$  was estimated from the best fit of the density profile and ii) by considering an energy threshold, i.e.  $e/e_0 < -20$  where  $e/e_0 = -20$  corresponds to the inner peak of  $p(e)$  and  $e_0$  is defined in Eq.4). In the latter case the fit is better than in the former one: we interpret this as due to the fact that the energy threshold selects the particles in the inner core better than the distance cut, as in that case particles that have higher energy and thus belong to the halo at a subsequent time can be confused with the core particles. The temperature  $T$  can be thought to be an effective temperature related to an isotropic and scale-independent velocity dispersion, i.e. it does not represent a real equilibrium thermodynamical temperature. Fig.3 (bottom panel) shows the almost flat density distribution in the central region where, additionally, the velocity distribution is isotropic.

Thermal equilibrium is reached in the core driven by two-body collisions. Indeed, the order of magnitude of the time scale for collisional relaxation is (Binney & Tremaine 2008)

$$\tau_{2b} \approx \frac{N}{\log N} \tau_{dyn} \approx \frac{N}{\log N} \sqrt{\frac{\rho}{\rho_0}} \tau_{ff} \quad (13)$$

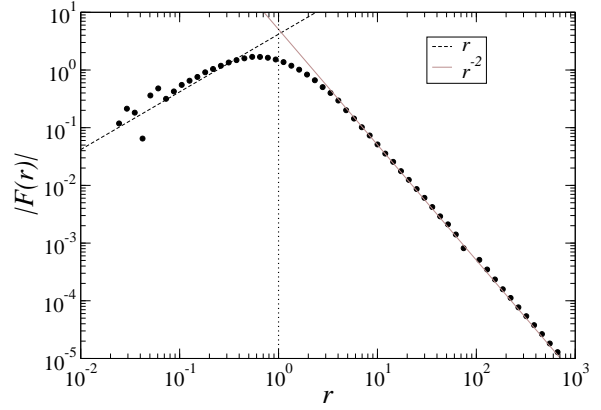


**Fig. 4.** Absolute value of the force as a function of scale in the QSS.

where  $\tau_{ff}$  is the free fall time of the system (that has initial density  $\rho$  — see Eq.1),  $\tau_{dyn} \sim (G\rho_0)^{-1/2}$  is the dynamical time of the core with density  $\rho_0 \gg \rho$ . In the core, i.e. for  $r < r_0$ , we find that  $\rho/\rho_0 \sim 10^{-5}$  and  $N/\log(N) \sim 10^2 - 10^3$  (log is the decimal logarithm) and thus  $\tau_{2b} \approx \tau_{ff}$ : two-body relaxation is efficient enough to establish thermal equilibrium in the core in a timescale of order of  $\tau_{ff}$ . Note that an approximate thermal equilibrium is reached in the short timescale corresponding to the global collapse of the system  $\tau_{dyn}$  and that on a much longer timescale, driven by two-body encounters; eventually the QSS that emerges from the violent relaxation process will undergo to a gravothermal collapse.

The power law fit to the density profile is very well defined for  $r \geq 4r_0$ : such a region contains most of the system's mass and it is surrounded by a lower density region of bound particles, still spherically symmetric distributed, in which the density displays a power-law decay and whose velocity distribution is radially biased. Given these conditions, we aim to find the relation between the exponent  $\alpha$  of the power-law fit to the density profile, i.e.  $\rho(r) \sim r^{-\alpha}$ , and the anisotropy parameter  $\beta(r)$  given that the Jeans equation (Eq.8) is satisfied. We note that, under the hypotheses mentioned above, the gravitational potential decays, for  $r > r_0$ , as  $\phi(r) \sim -GM_0/r$  — corresponding to a force that decays as  $r^{-2}$  (see Fig.4).

In this external zone, due to low density, the self-interaction between particles can be neglected so that the maximum speed of a particle at distance  $r$  is the local escape velocity, i.e.  $v_r^M(r) = \sqrt{GM_0/r}$  (see the upper panel of Fig.5).

By assuming that the probability distribution function (PDF) of  $v_r(r)$  is uniform in the range  $[-v_r^M(r), v_r^M(r)]$ , a situation that occurs if the system is virialized (see the middle panel of Fig.5), we find

$$\overline{v_r^2(r)} = \int_{-v_r^M(r)}^{v_r^M(r)} p(v_r) v_r^2 dv_r = \frac{1}{3} \frac{GM_0}{r} \quad (14)$$

The bottom panel of Fig.5 shows that Eq.14 well approximates the measured behaviors. From Eq.8 and Eq.14 we

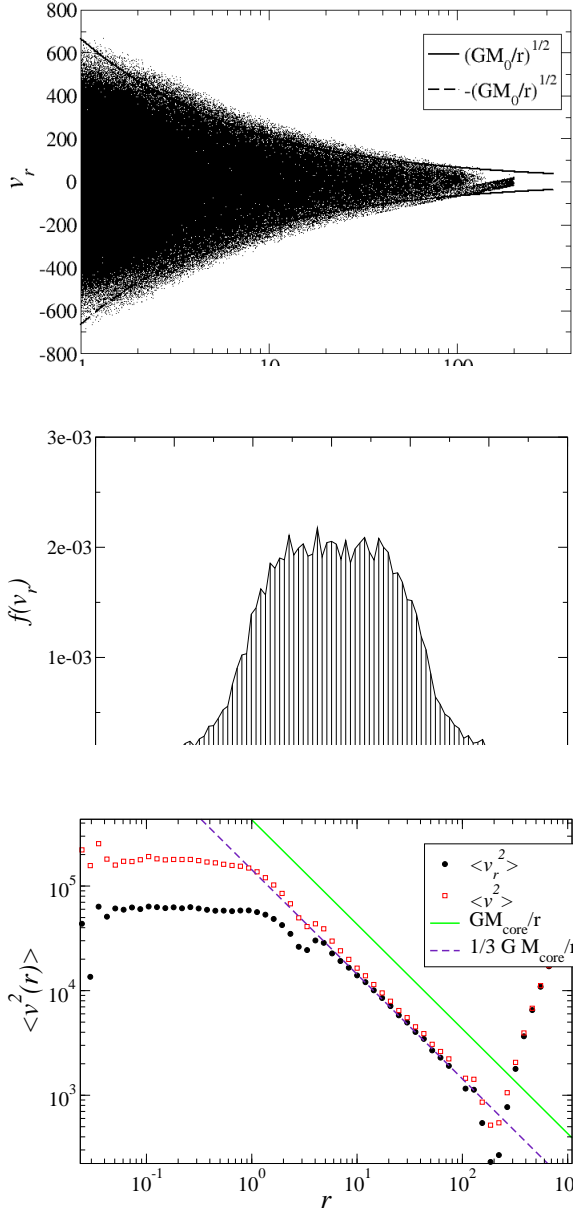


**Fig. 5.** Upper panel: The radial component of the velocity  $v_r$  as function of the distance for particles in the tail. Middle panel: example of the velocity distribution  $f(v_r)$  in a tail shell. Bottom panel:  $\langle v_r^2(r) \rangle$  and  $\langle v_r^2(r) \rangle$  as function of the radial distance

find that for  $r > r_0$

$$\frac{1}{\rho(r)} \frac{d\rho(r)}{dr} = \frac{1}{r} \left( \frac{\phi_0}{v_r^2(0)} + 1 - 2\beta(r) \right) = \frac{-2(1 + \beta(r))}{r}. \quad (15)$$

If we take  $\beta(r) = 1$  we find

$$\rho(r) \sim \frac{\rho_0}{r^4}, \quad (16)$$

that well approximates the power-law tail observed in numerical simulations, i.e. Eq.9.

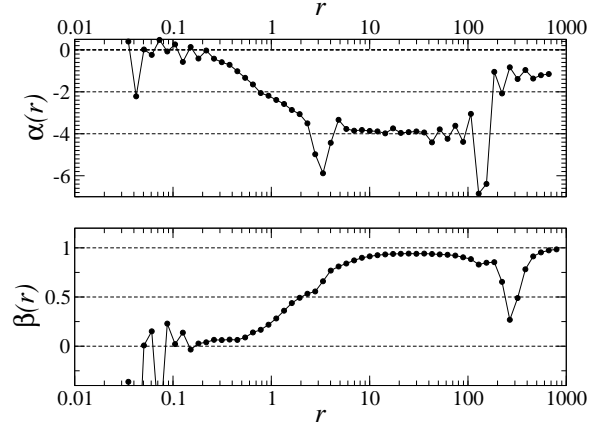


**Fig. 6.** Upper panel: radial behavior of the exponent  $\alpha(r)$  of the density profile. Bottom panel: radial behavior of the anisotropy parameter  $\beta(r)$ .

In these same approximations we find, for  $r \gg r_0$

$$\alpha \approx 2(1 + \beta) \rightarrow 4 \text{ for } \beta \rightarrow 1. \quad (17)$$

However, one should be careful in extrapolating Eq.17 for any value of  $\beta, \alpha$ : indeed, in general the situation is more complicated as neither Eq.14 nor  $|\phi| \sim 1/r$  is satisfied when the density decays slower than  $r^{-4}$  and one should consider Eq.8 instead of Eq.17 and thus  $\alpha$  is expected to have a non-trivial dependence on  $\beta$  and on the whole mass distribution.

In summary, in the case of a violent relaxation of an isolated, cold, spherically symmetric, uniform mass distribution we have obtained the limiting behaviors (see Fig.6)

$$\alpha \rightarrow 0 \text{ for } \beta \rightarrow 0 \text{ } r \leq r_0 \quad (18)$$

$$\alpha \rightarrow 2(1 + \beta) \text{ for } \beta \rightarrow 1 \text{ } r \gg r_0.$$

### 3.4. Isolated spherical over-densities with non-Poissonian fluctuations

As discussed Sect.2 the key parameter of the second family of IC is  $\gamma$  (see Eq.2): when  $\gamma = 10$  the number of centers is only ten times less than the number of particles, and thus fluctuations are slightly greater than in the purely Poissonian case. On the contrary, when  $\gamma \approx 10^5$  the IC consist of sub-clumps that have collapse timescales shorter than that of the system as a whole. In this situation sub-clumps collapse almost independently from each other and, then, the different sub-structures merge. A separation of spatial and temporal scales occurs only when the IC is highly inhomogeneous, i.e. few centers. The intermediate range for  $\gamma$ ,  $10 < \gamma < 10^5$ , is the most interesting to study.

Figure 7 shows the behavior of the quantity  $\Delta(t)$ , defined by Eq.3, that measures the amount of energy exchanged among system particles: there is a clear trend showing that the more uniform is the IC the larger is the energy variation. This trend is in line with the Poissonian

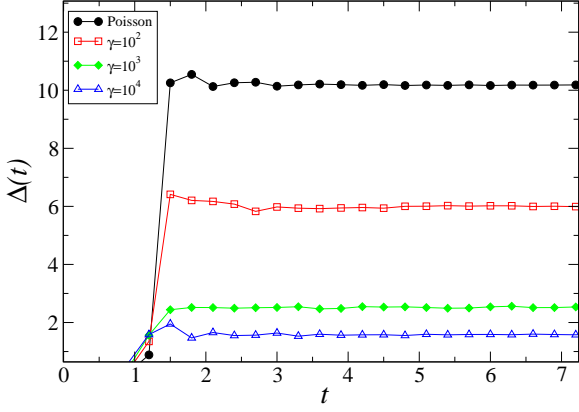


**Fig. 7.** Behavior with time of the quantity  $\Delta(t)$  (see Eq.3) in simulations of isolated spherical over-densities with non-Poissonian fluctuations with different values of  $\gamma$ . The behavior for the case of the initially Poissonian spherical

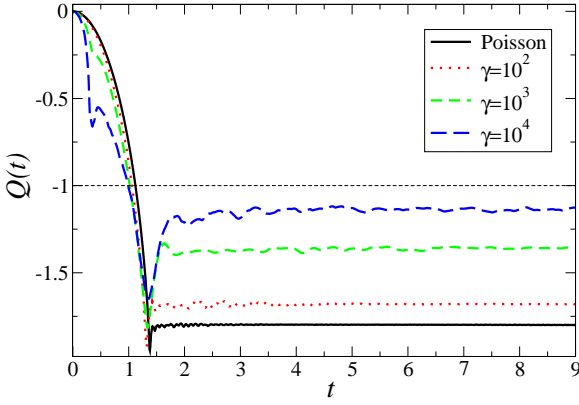


**Fig. 8.** Time evolution of the virial ratio  $Q$  in simulations of isolated spherical over-densities with non-Poissonian fluctuations with different  $\gamma$ . The case of the initially Poissonian spherical over-density is also shown for comparison (in black).

case, where the larger is  $N$ , the smaller the initial fluctuations over the mean and the larger the variation of  $\Delta(t)$  (Joyce et al. 2009). Consequently the asymptotic value of the virial ratio becomes the closer to  $-1$  the smaller is the energy exchange and thus the smaller the amount of particles that have been ejected from the system after the collapse (see Fig.8). The reflection of this situation can be clearly seen in the asymptotic shape of the particle energy distribution (see Fig.9): the more clustered is the initial distribution, the softer the collapse and the less spread is  $p(e)$  after the collapse.

The density profiles of the QSS in the various simulations are shown by Fig.10: while there is a clear change of slope in all cases between the inner core and the outer regions, the softer is the collapse and the less marked is such a change. That is, while for the uniform case there is a clear change from  $n(r) \sim \text{const.}$  in the inner core to  $n(r) \sim r^{-4}$  in the outer regions, when the initial fluctuations are large enough, i.e.  $\gamma \approx 10^2 - 10^4$ , then the density

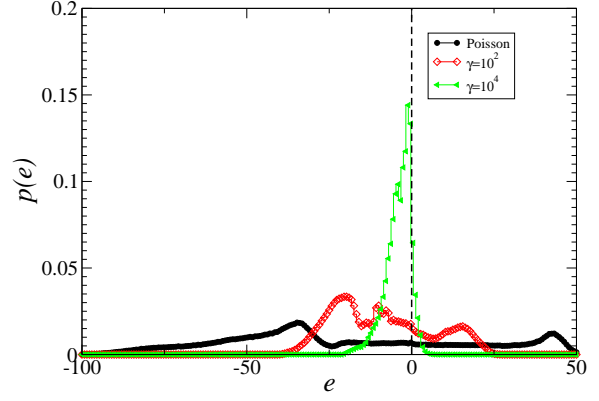


**Fig. 9.** Asymptotic particle energy distribution in the two non-Poissonian simulations. The case of a Poissonian IC

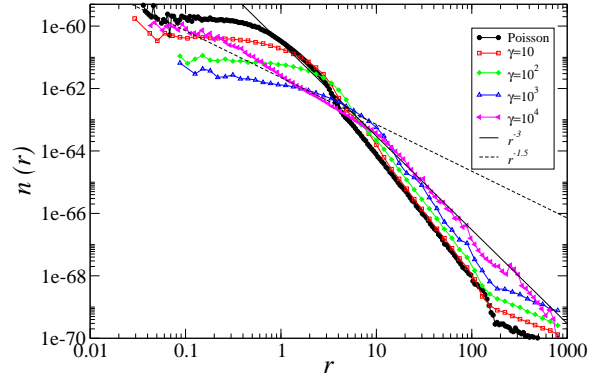


**Fig. 10.** Density profile in the three simulations of isolated spherical over-densities with non-Poissonian fluctuations with different  $\gamma$ . The behavior for the case of the initially Poissonian spherical over-density is also shown for comparison (in black).

profile in the inner core is closer to  $n(r) \sim r^{-1}$  and in the outer region to  $n(r) \sim r^{-3}$ .

The QSS formed are close to Jeans's equilibrium in all cases: we find that  $\psi(r) \approx 1$  in an intermediate range of scales between the inner regions where shot noise fluctuations are predominant and the outermost regions where particles have positive energy.

In order to clarify the statistical and dynamical properties of the QSS let us focus on the case in which initial fluctuations are large but the number of sub-clusters is still large enough so that they have a substantial overlap and thus there is not a separation of length and time scales in the collapsing phases of the whole structure and of its substructures. We thus focus on the case  $\gamma = 10^4$ .

Fig.11 shows the velocity dispersions as a function of distance to the centre in the asymptotic QSS. One may identify three different regimes that correspond to:

- (i) an inner region where the dispersion slightly grow inward in an almost isotropic manner, i.e.  $\langle v_t^2 \rangle \approx 2\langle v_r^2 \rangle$ , corresponding to  $\beta(r) \approx 0$ ,



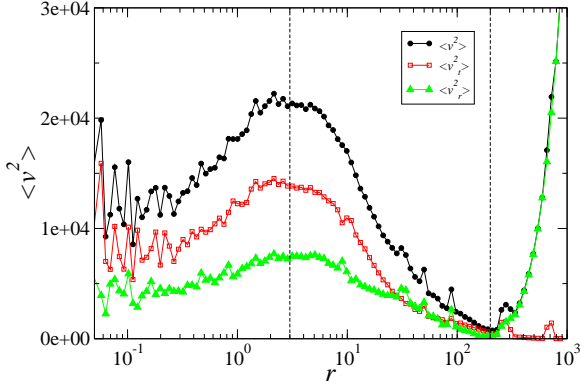


**Fig. 11.** Velocity dispersion (total, transverse and radial) as a function of distance in the asymptotic QSS for a the

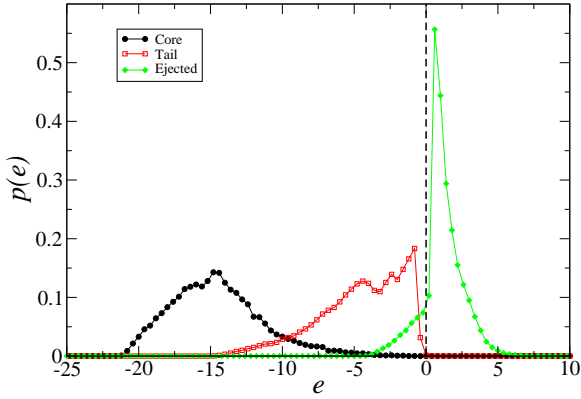
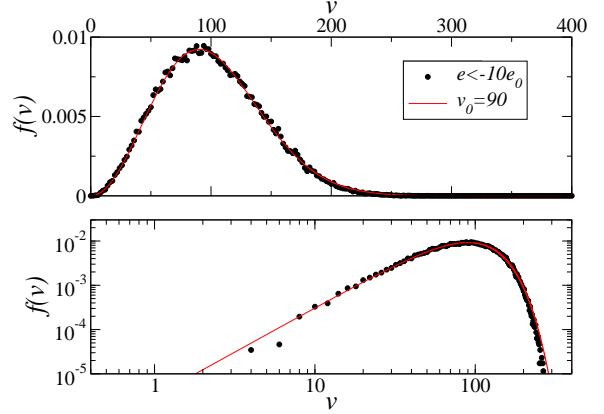


**Fig. 12.** Particle energy distribution in the asymptotic QSS for the case of a very clustered IC, i.e.  $\gamma = 10^4$

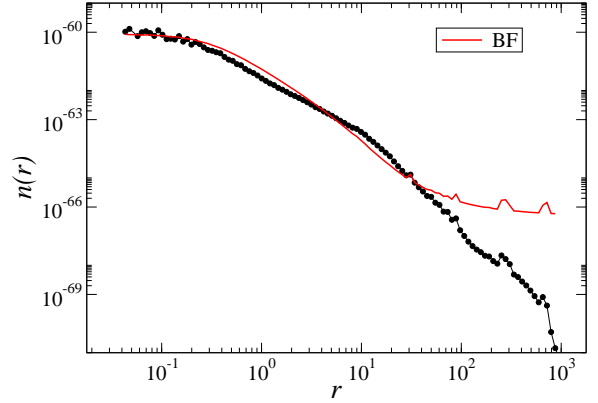
- (ii) a tail where the dispersion (in all components) decreases as a function of the radial distance and  $\langle v_r^2 \rangle > \langle v_t^2 \rangle$ ,
- (iii) an outermost regions where  $\langle v_t^2 \rangle \approx 0$ , that is where highly energetic particles move on quasi-radial orbits.

Figure 12 shows the particle energy distribution: particles in the core are selected as those having  $r < r_0$ , where in this case  $r_0$  approximately coincides with the peak of  $\langle v^2(r) \rangle$  (see Fig. 11) and the ejected particles have  $r > r_f$  where  $r_f$  is estimated to be the (time dependent) scale at which  $\langle v^2(r) \rangle \approx \langle v_r^2(r) \rangle$ . The core is populated by the most bound particles, the tail is made by particles with slightly negative energy, while particles in the outermost region have  $e > 0$ .

Figure 13 shows the velocity distribution of the particles in the core region. As for the case of the Poissonian IC, a Maxwell Boltzmann distribution represents here a good fit, clearly at a much lower “temperature” (i.e. velocity dispersion) than for the uniform case. The selection of the inner regions has been done in two ways: by considering a limit in radial distance (i.e.,  $r < r_0$ ) and a limit in energy ( $e < -10e_0$ ). In the latter case the MB distribution fit better interpolates the data. In the inner core thermal



**Fig. 13.** Velocity distribution of the inner regions of the asymptotic QSS for a the case of a very clustered IC, i.e.  $\gamma = 10^4$ . The selection has been performed in energy (i.e.,  $e < 10e_0$ ): the best-fitting Maxwell-Boltzmann distribu-



**Fig. 14.** Density profile in the inner core of the asymptotic QSS for a the case of a very clustered IC, i.e.  $\gamma = 10^4$ : the best-fitting with Eq. 12 is also shown.

equilibrium is reached driven by two-body collisions even in this case.

Figure 14 shows the density profile in the inner region for  $\gamma = 10^4$ : even in this case, the density distribution is here well described by Eq. 12. Figure 15 shows the behavior of the anisotropy parameter  $\beta(r)$  (bottom panel) and of the exponent of the density profile  $\alpha(r)$  (upper panel) as functions of the distance from the center: notice that, like in the case of the cold uniform spherical over-density,  $\beta(r) \rightarrow 0$  in the core and  $\beta(r) \rightarrow 1$  in the outermost region; correspondingly the exponent of the density profile  $\alpha \rightarrow 0$  in the core and  $\alpha \rightarrow -4$  in the tail. Beyond these two limiting cases it is not possible to obtain an analytical expression of  $\alpha(\beta)$  for the general case. Indeed, the actual mass distribution is more spread than in the simplest model where  $\rho \sim \text{const.}$  in the inner region and  $\rho \sim r^{-4}$  in the outer tail. This is quantitatively illustrated by the behavior of the gravitational force in models with different values of  $\gamma$  (see Fig. 16): at short distances from the centre the linear growth (implied by a constant mat-

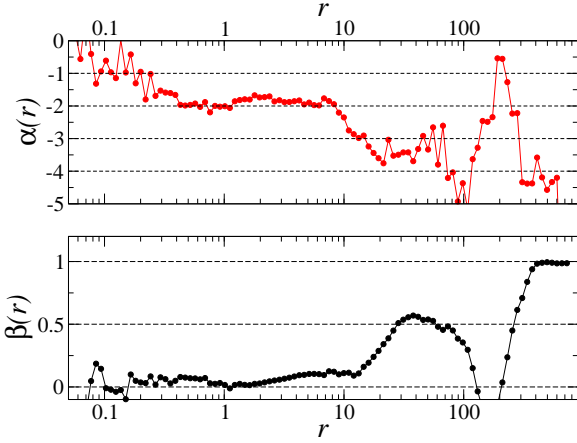


**Fig. 15.** Upper panel: behavior of the exponent of the density profile  $\alpha(r)$  of a QSS with  $\gamma = 10^4$ . Bottom panel: behavior of the anisotropy parameter  $\beta(r)$  as a function

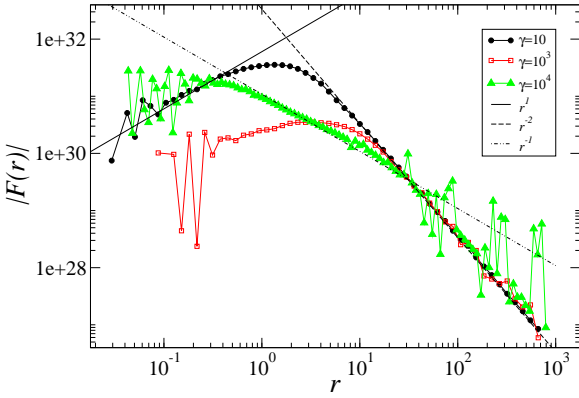


**Fig. 16.** Absolute value of the gravitational force as a function of function of scale in the QSS in simulations with different values of  $\gamma$ .

ter density) is clear only when  $\gamma < 10^3$ . For large  $\gamma$ , for instance  $\gamma = 10^4$ , the force has a short range of radial growth to decay after as  $r^{-1}$  in a intermediate range of distance scales.

### 3.5. Cosmological halos

As mentioned in Sect.2 we have also considered a set of data extracted from the Abacus simulations (Garrison et al. 2018, 2019) representing the so-called halos typical of cosmological simulations. Their shape is typically ellipsoidal and are characterized by several substructures. Nevertheless, we treat these systems in spherical symmetry, as the ratio between the axis is close to one, and we compute the center as the minimum of the potential energy. A certain degree of arbitrariness in the definition of the outermost cut-off of a halo is present. Here, we just consider the outputs of the Abacus halo finder keeping in mind that faraway low density particles with high energy maybe not included because of a selection effect.

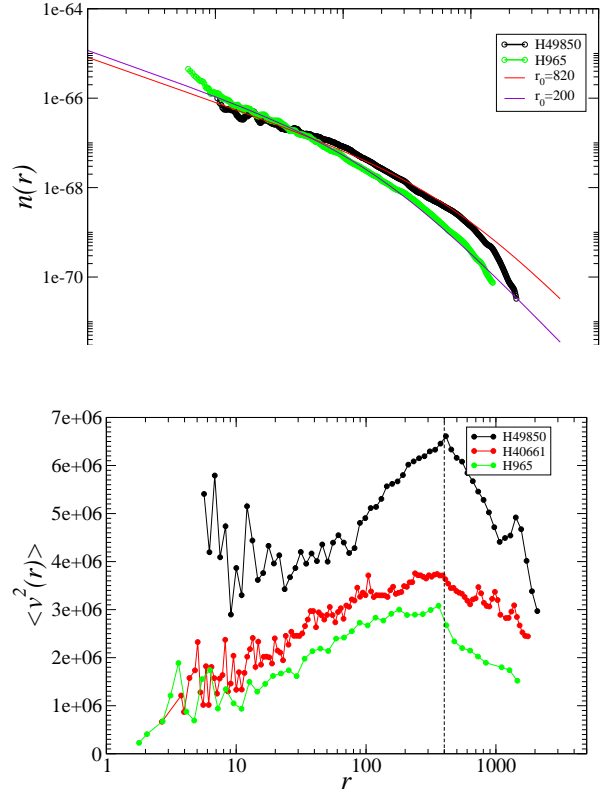


**Fig. 17.** Upper panel: Density profile in two of most massive halos. The two solid lines represent the best fit respectively for H49850 and H965 with a NFW profile. Bottom panel: the velocity dispersion  $\langle v^2(r) \rangle$  for the same halos together with H40661.

In what follows, we report results for the three more massive halos H49850, H40661 and H965 that contain, respectively,  $\sim (8, 4, 3) \times 10^5$  particles. We checked that, when considering smaller halos the results do not qualitatively change but the statistical estimators are noisier.

The density profiles of two halos are shown in upper panel of Fig.17. The density profile slope changes from  $\alpha \approx -1$  in the inner region to  $\alpha = -2$  in the outer region of the system. The NFW profile (see Eq.10) provides good fits of the behaviors but in the outermost part of the tail, where, as we noticed, there is some arbitrariness in the definition of the particle memberships. The radial behavior of the average square velocity resembles that observed in isolated spherical collapse models with non-Poissonian fluctuations (see Fig.11): indeed,  $\langle v^2(r) \rangle$  grows with distance reaching a maximum at  $\sim r_0$  and then it decays at large distances. The radial and transverse velocity dispersion (not plotted) display a similar behavior. The radial scale  $r_0$  roughly separates the two regimes.

The particle energy distribution is shown in Fig.18: a small fraction of the particles has positive energy in all the three cases: this fraction clearly depends on the manner the external part of the halos has been selected. Differently from Fig.2 and Fig.9 in this case the energy is normalized to  $e_0 = Wm/M$ , where  $W$  is the gravitational potential energy of the system at redshift  $z = 0$  (i.e., not the ini-

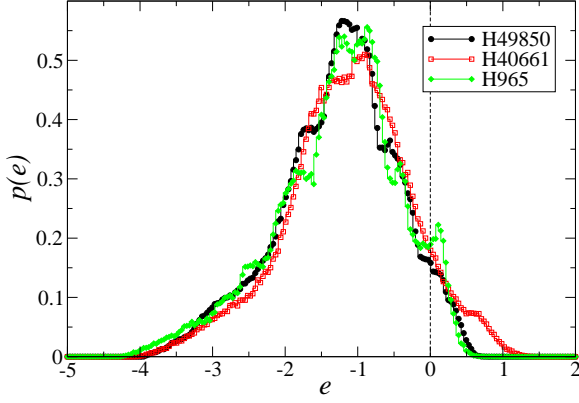


**Fig. 18.** Particle energy distribution in the three largest Abacus halos. In this case the energy is normalized to  $e_0 = Wm/M$  where  $W$  is the total gravitational potential energy of the system at  $z = 0$  (i.e., not the initial one)  $M$

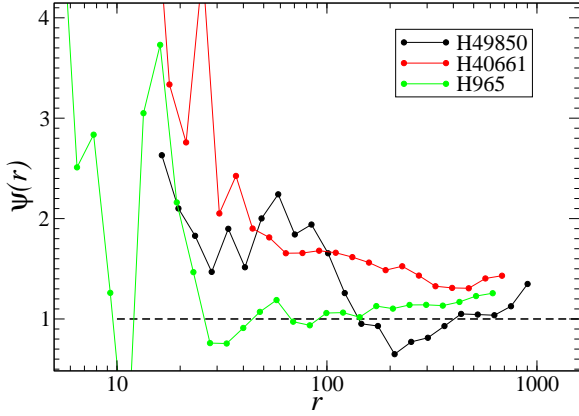


**Fig. 19.** Behavior of the parameter  $\psi(r)$  (see Eq.8) for the three largest Abacus halos.

tial),  $M$  its mass and  $m$  the particle mass: this is clearly much larger (in absolute value) than the initial one. Note that we treat each halo as being isolated: this is clearly an approximation which works better the larger is the halo density contrast.

The overall shape of these  $p(e)$  is very similar to those obtained in the case of isolated spherical collapse models with non-Poissonian fluctuations and large  $\gamma$ . (see Fig.9).

The halos are close to an equilibrium condition as described by the Jeans equation (see Eq.8), i.e.  $\psi(r) \approx 1$  (see Fig.19): at small distances  $\psi(r)$  has shot-noise fluctuations while the outermost region of the tail is out-of-equilibrium as particles have positive energy. In the intermediate region  $\psi(r)$  presents larger fluctuations than for the case of the uniform sphere (Fig.1): this is probably due to the presence of more substructures and to the influence of neighboring density perturbations, as now these over-densities are not isolated as in the previous cases.

The inner region shows the velocity distribution that is well approximated by a MB distribution (see Fig.20). Inner region particles were selected by considering a radial

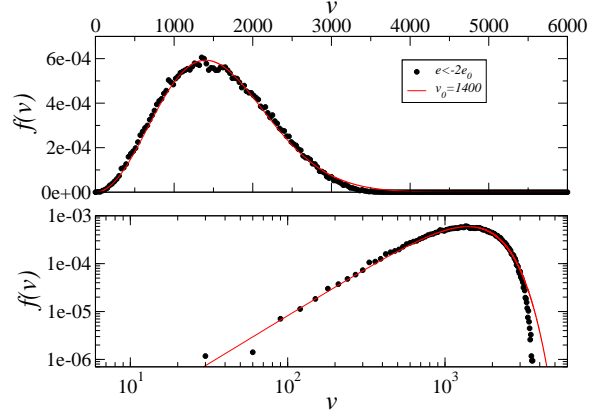


**Fig. 20.** Velocity distribution in the inner core for the most massive Abacus halo (i.e., H49850) together with the best fit with a Maxwell-Boltzmann distribution. Inner region particles were selected by considering an energy cut ( $e < 2e_0$ )

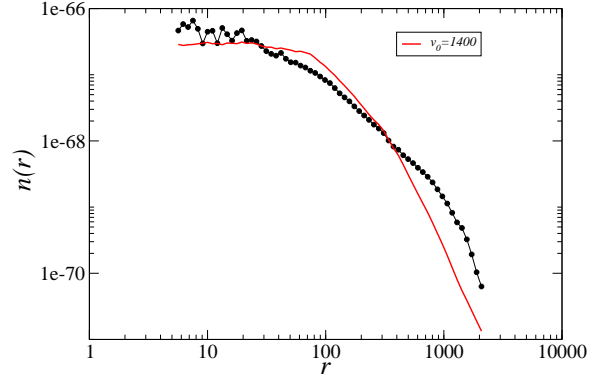
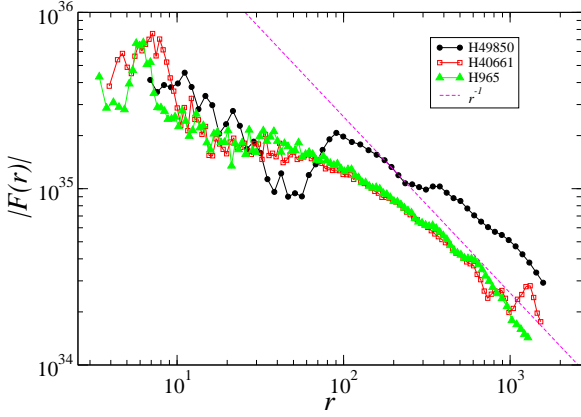


**Fig. 21.** Density profile of the most massive Abacus halo (i.e., H49850). The best-fitting with Eq.12 is also shown

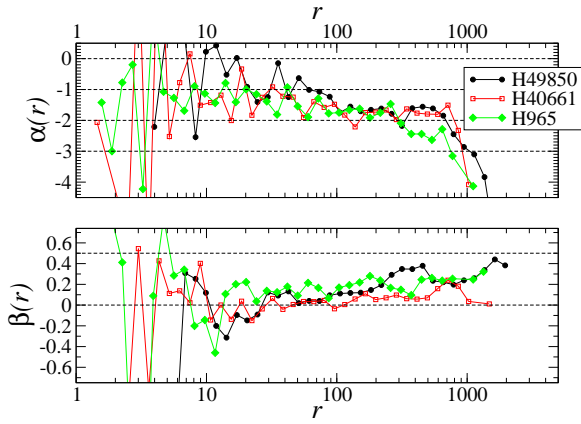
distance cut (i.e.,  $r < r_0$ ) and, alternatively, an energy cut: in the latter case the MB distribution fits better the data, as for the cases of Fig.3 and Fig.13. If we use Eq.12 to compute the density profile of the inner region we obtain a fit worse than in the cases discussed previously (see Fig.21) but still reasonably good. On the other side, the fit is particularly rough at large radial distances: this is probably due to that the halo is not actually isolated in these simulations system.

Figure 22 shows the behavior of the absolute value of the gravitational force in the three examined massive halos: this is approximately constant at small radii and then it decays as  $\sim r^{-1}$  at large distances, a behavior consistent with the density profile shown in Fig.17. The large fluctuations in the force profile, especially for the case of the halo H49850, are due to sub-structures.

Finally, the anisotropy parameter (bottom panel of Fig. 23) is  $\beta \approx 0$  in the inner zone (where  $n(r) \sim r^{-1}$ ) while  $\beta \approx 0.5$  in the outer regions of the system (where  $n(r) \sim r^{-2}$ ).



**Fig. 22.** Absolute value of the force as a function of function of scale in the Abacus halos



**Fig. 23.** Upper panel: derivative of the density profile for the three largest Abacus halos. Bottom panel: anisotropy parameter.

### 3.6. Discussion

In high-resolution simulations of CDM halos it was noticed (Taylor & Navarro 2001) that the coarse-grained phase-space density decays as

$$\frac{\rho(r)}{\langle v_r^2(r) \rangle^{3/2}} \sim \frac{1}{r^\mu}, \quad (19)$$

where  $\mu \approx 1.875$ . We compare results of our experiment with the above behavior, starting from the violent collapse case of a uniform sphere. In this case, combining Eq.9 and Eq.14 we find  $\mu = 5/2$  in the tail, while in the core  $\mu \simeq 0$  (see upper panel of Fig. 24). The QSS established after the collapse of spherical distributions with non-Poissonian fluctuations show a behavior that depends on the parameter  $\gamma$ : when  $\gamma$  is small, and thus the initial fluctuations are close to Poissonian, then the slope  $\mu$  is similar to the that of the Poissonian case. When instead the distribution is initially clustered, i.e.,  $\gamma = 10^3 - 10^4$ , then the slope is  $\mu \approx 1.875$  (see the middle panel of Fig. 24).

The different behavior observed for the isolated and clustered simulations in function of  $\gamma$  is again a good evidence that by changing such a parameter the mean-field and collisionless dynamics that drive system to reach a

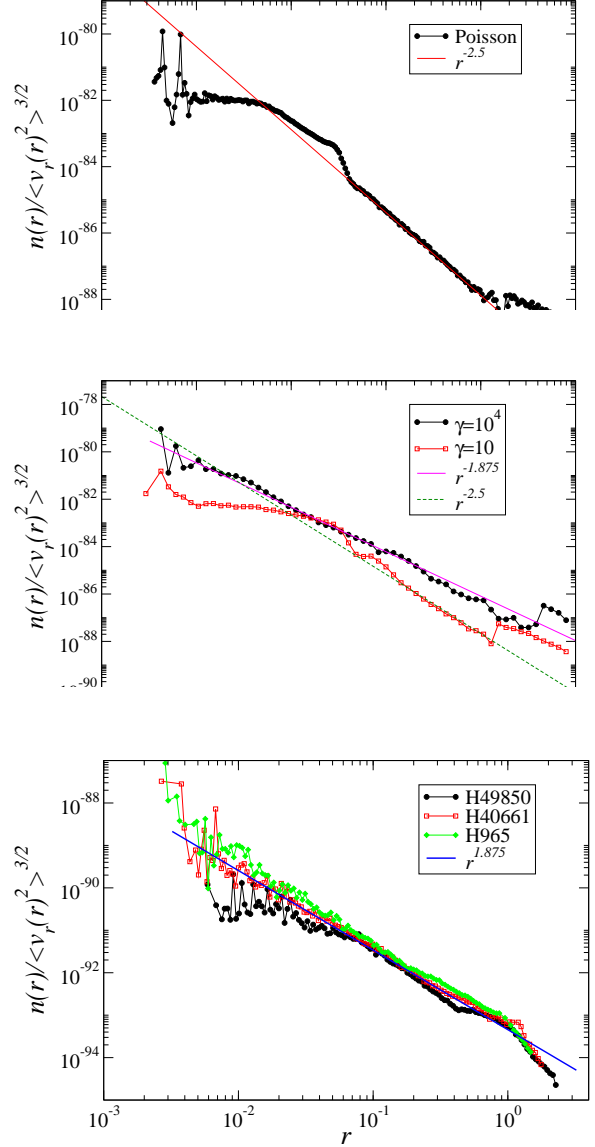


**Fig. 24.** Coarse-grained phase-space density in the uniform case (upper panel), non-uniform case (middle panel) and cosmological halos (bottom panel).

QSS passes from being close to a top-down monolithic collapse to a bottom-up hierarchical aggregation process. Finally, in the cosmological halos of the previous subsection we find  $\mu \approx 1.875$ , thus very similar to the isolated case with  $\gamma = 10^3 - 10^4$  (see the bottom panel of Fig.24).

For the case of cosmological halos, there have been attempts to determine the slope of the density profile  $\alpha$  for spherically symmetric and *isotropic* systems that are in Jeans equilibrium and that exhibit power-law coarse-grained phase-space density (Taylor & Navarro 2001). It was formally shown that the allowed density slopes  $\alpha$  lie in the range  $[1, 3]$  (Hansen 2004). It was then noticed that, in halos extracted from cosmological simulations, there a linear relationship between the density slope and the anisotropy parameter (Hansen & Moore 2006;



Hansen & Stadel 2006; Hansen et al. 2006), although with a large scattering, where for  $\alpha \rightarrow 3$  for  $\beta \rightarrow 0.5$  and  $\alpha \rightarrow 1$  for  $\beta \rightarrow 0$ . These trends are similar to what we obtain examining the Abacus halos but not for case in which the more violent relaxation occurring when a monolithic collapse takes place as in this latter case  $\alpha \rightarrow 0$  for  $\beta \rightarrow 0$ . This situation thus shows that the relation between  $\alpha$  and  $\beta$  is determined by the dynamical mechanism at work rather being universal as argued by (Hansen & Moore 2006).

From an analytical point of view, by using the hypotheses that both the coarse-grained phase-space density and the density profile being a power-law in distance allowing for the possibility that the velocity distribution is not isotropic and the empirical linear relation between  $\alpha$  and  $\beta$ , it is possible to solve the Jeans equations analytically and extract the relevant statistical information of the system (Dehnen & McLaughlin 2005). However, a purely power-law coarse-grained phase-space density approximates well the observed behavior only for the case of a bottom-up dynamics but not for the top-down one.

#### 4. Conclusions

Two competing processes work to determine the dynamical evolution of finite initially spherical and cold self-gravitating systems: on one hand they undergo to a global (top-down) collapse driven by their own rapidly varying gravitational field, and, on the other hand, internal density fluctuations lead to formation of local substructures of growing size through a (bottom-up) aggregation process. Therefore, in general, there is a sort of competition between a top-down and a bottom-up mean-field collisionless dynamics. Anyway, in both cases collisional effects are negligible because of their much longer time scale respect to that giving rise to quasi-stationary states (QSS).

The properties of the QSS formed depend on the evolutionary paths they have followed, and thus on which of the above mentioned two mechanisms prevails during the relaxation from the out-of-equilibrium IC to the quasi-stationary configuration. In particular, the dynamics is different depending on the type of correlation properties between initial density perturbations. When the amplitude of initial fluctuations is small, a global collapse takes place and the system relaxes into a QSS in a very short time: the signature of this process is a wide energy exchange between particles. On the other hand, in case of large initial fluctuations, the bottom-up aggregation process becomes predominant over the global collapse and, so, clustering at small scales builds up larger and larger substructures halting, actually, the global collapse. That is, the fragmentation into large and growing sub-structures inhibits the occurrence of a large variation of the overall system size and, consequently, the particle energy distribution only moderately changes.

We have considered a family of simple IC representing isolated, spherical and ‘cold’ distributions of particles with different spectra of initial density fluctuations. By varying

the initial amplitude of initial density perturbations we find that it is possible to select the mechanism through which the out-of-equilibrium IC are driven to form a QSS.

As we said above, for the case of a top-down (monolithic) collapse which occurs whenever the amplitude of initial density fluctuations are small, the particle energy distribution changes significantly in a rapid interval of time centered around the time of maximum system contraction (essentially the free-fall time): such variation is given by the interplay of the finite size of the system with the growth of density perturbations during the collapse. In this situation, the QSS are characterized by a compact core, that contains a significant fraction of the system mass and that shows an almost isotropic velocity distribution. The core is surrounded by a low density region where orbits are quite elongated, i.e. where the velocity anisotropy parameter  $\beta$  tends to 1. By an argument based on the assumption of validity of the Jeans equation, we were able to show that the inner region of a system emerging by a violent top-down collapse is characterized by an almost flat density profile while the outer power law decay of density is  $\rho(r) \sim r^{-4}$ , a behavior that is actually observed in the numerical experiments of initially cold and uniform systems.

On the other hand, when initial perturbations are of large enough amplitude then a quasi-stationary state is reached through a bottom-up, hierarchical, aggregation process: small sub-structures merge to form larger and larger ones. This process is accelerated when initial density correlations are long-range. That is, at given initial fluctuations amplitude, the smaller the power-law index  $n \in (-3, 0]$  of the density fluctuation power spectrum  $P(k) \sim k^n$  the faster the evolution of the bottom-up mechanism of structure formation. In this latter situation, the variation of the particle energy distribution is smaller than in the former and, for this reason, the orbits in the outermost regions of the system are less radially elongated. The exponent of the density profile is  $0 < \alpha \leq 4$  and the anisotropy parameter is  $0 \leq \beta < 1$ . When initial density perturbations are large enough the core-halo structure is not formed. In this case the profile is better fitted by a NFW behavior.

We have also demonstrated that the halos formed in cosmological  $N$ -body simulations in the standard CDM scenario, although they are not isolated but rather embedded in the tidal field of neighboring structures, show properties similar to QSS obtained in the simple isolated and spherical cases considered here, in the case of large enough initial fluctuation amplitudes. Indeed, in CDM-like cosmologies, density fluctuations are long-range correlated (i.e.,  $P(k) \sim k^{-2}$ ) and, as said above, this situation implies the development of a bottom-up aggregation process rather than a top-down scenario through the collapse of large over-densities. We can thus conclude that isolated, spherical and dynamically cold systems with different choices of initial density perturbations amplitude represent a useful tool to study the formation of QSS through a mean-field collisionless dynamics, both when

the clustering proceeds in a bottom-up and in a top-down way. The fact that systems emerging from cosmological environment have similar properties to those emerging from isolated IC imply that, when fluctuations are highly non-linear, the evolution of a cosmological halo is well approximated by neglecting tidal interactions with neighboring structures.

To conclude, let us now consider a long-standing observational puzzle that can be related with these results. This is the *core-cusp* problem, i.e. the well known difference between the observed inner density profiles of dark matter in low-mass galaxies and the density profiles obtained in cosmological  $N$ -body simulations. Observations seem to indicate an approximately constant dark matter density in the inner parts of galaxies (a core), while CDM halos profiles show instead a  $\sim r^{-1}$  power-law cusp at short distances (Navarro et al. 1997). This fact, known as the core/cusp controversy, stands as one of the unsolved problems in small-scale cosmology (see for a recent review De Blok (2010) and references therein). Our results suggest that a possible solution of this puzzle could be found in a violent origin of the galaxies, i.e. through something more similar to a monolithic collapse than to a bottom-up aggregation process. We refer the interested reader to (Benhaïem et al. 2017, 2019; Sylos Labini et al. 2020) for further discussions of this specific topic. Concerning the latter point we note that the case for galaxy formation through a monolithic collapse has been very recently advocated also by Peebles (2020).

## Acknowledgements

We are grateful to Lehman Garrison for his valuable assistance in explaining us the Abacus database and for providing us an ad-hoc simulation with high resolution halos catalogs and data. The Abacus data are available at <https://lgarrison.github.io/AbacusCosmos/>. We are grateful to Volker Springel for his help in the use of Gadget-2.

## References

- Aarseth, S., Lin, D., & Papaloizou, J. 1988, *Astrophys. J.*, 324, 288
- Aguilar, L. & Merritt, D. 1990, *Astrophys. J.*, 354, 73
- Arca-Sedda, M. & Capuzzo-Dolcetta, R. 2014, *Astrophys. J.*, 785, 51
- Barnes, E. I., Lanzel, P. A., & Williams, L. L. R. 2009, *Astrophys. J.*, 704, 372
- Baushev, A. & Barkov, M. 2018, *Journal of Cosmology and Astroparticle Physics*, 2018, 034034
- Benetti, F. P. C., Ribeiro-Teixeira, A. C., Pakter, R., & Levin, Y. 2014, *Phys. Rev. Lett.*, 113, 100602
- Benhaïem, D., Joyce, M., & Sylos Labini, F. 2017, *Astrophys. J.*, 851, 19
- Benhaïem, D., Joyce, M., Sylos Labini, F., & Worrakitpoonpon, T. 2016, *Astron. Astrophys.*, 585, A139
- Benhaïem, D. & Sylos Labini, F. 2015, *Mon. Not. R. Astron. Soc.*, 448, 2634
- Benhaïem, D. & Sylos Labini, F. 2017, *Astron. Astrophys.*, 598, A95
- Benhaïem, D., Sylos Labini, F., & Joyce, M. 2019, *Phys. Rev. E*, 99, 022125
- Binney, J. & Knebe, A. 2001, *Mon. Not. Roy. Astron. Soc.*, 325, 845
- Binney, J. & Tremaine, S. 2008, *Galactic Dynamics* (Princeton University Press)
- Blumenthal, G. R., Faber, S. M., Primack, J. R., & Rees, M. J. 1984, *Nature*, 311, 517
- Blumenthal, G. R., Pagels, H., & Primack, J. R. 1982, *Nature*, 299, 37
- Boily, C., Athanassoula, E., & Kroupa, P. 2002, *Mon. Not. R. Astr. Soc.*, 332, 971
- Boily, C. M. & Athanassoula, E. 2006, *Mon. Not. R. Astr. Soc.*, 369, 608
- Bond, J. R., Szalay, A. S., & Turner, M. S. 1982, *Phys. Rev. Lett.*, 48, 1636
- Campa, A., Dauxois, T., Fanelli, D., & Ruffo, S. 2014, *Physics of Long-Range Interacting Systems* (Oxford)
- Capuzzo-Dolcetta, R. A. 2019, *Classical Newtonian Gravity* (Springer International Publishing)
- Dauxois, T., Ruffo, S., Arimondo, E., & Wilkens, M. 2002, *Dynamics and Thermodynamics of Systems with Long-Range Interactions: An Introduction* (Berlin, Heidelberg: Springer Berlin Heidelberg), 1–19
- De Blok, W. J. G. 2010, *Advances in Astronomy*, 2010, 789293
- Dehnen, W. 1993, *Mon. Not. R. Astron. Soc.*, 265, 250
- Dehnen, W. & McLaughlin, D. E. 2005, *Monthly Notices of the Royal Astronomical Society*, 363, 10571068
- Diemand, J., Moore, B., Stadel, J., & Kazantzidis, S. 2004, *Mon. Not. Roy. Astron. Soc.*, 348, 977
- Garrison, L. H., Eisenstein, D. J., Ferrer, D., et al. 2018, *The Astrophysical Journal Supplement Series*, 236, 43
- Garrison, L. H., Eisenstein, D. J., & Pinto, P. A. 2019, *Monthly Notices of the Royal Astronomical Society*, 485, 33703377
- Hansen, S., Moore, B., & Stadel, J. 2006, *EAS Publications Series*, 20, 3336
- Hansen, S. H. 2004, *Monthly Notices of the Royal Astronomical Society*, 352, L41
- Hansen, S. H. & Moore, B. 2006, *New Astronomy*, 11, 333338
- Hansen, S. H. & Stadel, J. 2006, *Journal of Cosmology and Astroparticle Physics*, 2006, 014014
- Henon, M. 1964, *Ann. Astrophys.*, 27, 1
- Jeans, J. H. 1915, *Mon. Not. R. Astron. Soc.*, 76, 70
- Joyce, M., Marcos, B., & Sylos Labini, F. 2009, *Mon. Not. R. Astron. Soc.*, 397, 775
- Joyce, M. & Sylos Labini, F. 2013, *Mon. Not. R. Astron. Soc.*, 429, 1088
- Levin, Y., Pakter, R., & Rizzato, F. 2008, *Phys. Rev.*, E78, 021130
- Levin, Y., Pakter, R., Rizzato, F. B., Teles, T. N., & Benetti, F. P. 2014, *Physics Reports*, 535, 1, nonequi-

librium statistical mechanics of systems with long-range interactions

- Lynden-Bell, D. 1967, Mon. Not. R. Astr. Soc., 136, 101
- Merritt, D. & Aguilar, L. A. 1985, Mon. Not. R. Astr. Soc., 217, 787
- Navarro, J. F., Frenk, C. S., & White, S. D. M. 1997, Astrophys.J., 490, 493
- Navarro, J. F., Hayashi, E., Power, C., et al. 2004, Monthly Notices of the Royal Astronomical Society, 349, 1039
- Padmanabhan, T. 1990, Phys. Rept., 188, 285
- Peebles, P. J. E. 1980, The Large-Scale Structure of the Universe (Princeton University Press)
- Peebles, P. J. E. 2020, arXiv:2005.07588
- Roy, F. & Perez, J. 2004, Mon. Not. R. Astr. Soc., 348, 62
- Sahni, V. & Coles, P. 1995, Physics Reports, 262, 1
- Spera, M. & Capuzzo-Dolcetta, R. 2017, Astrophys. Space Sci., 362, 233
- Springel, V. 2005, Mon.Not.R.Astron.Soc., 364, 1105
- Sylos Labini, F. 2012, Mon. Not. R. Astron. Soc., 423, 1610
- Sylos Labini, F. 2013a, Astron. Astrophys., 552, A36
- Sylos Labini, F. 2013b, Mon. Not. R. Astron. Soc., 429, 679
- Sylos Labini, F., Benhaïem, D., & Joyce, M. 2015, Mon.Not.R.Astron.Soc., 449, 4458
- Sylos Labini, F., Pinto, L. D., & Capuzzo-Dolcetta, R. 2020, Physical Review E in the press, arXiv:2008.02605
- Taylor, J. E. & Navarro, J. F. 2001, The Astrophysical Journal, 563, 483
- Theis, C. & Spurzem, R. 1999, Astron. Astrophys., 341, 361
- van Albada, T. 1982, Mon. Not. R. Astr. Soc., 201, 939
- Worrakitpoonpon, T. 2015, Mon. Not. R. Astr. Soc., 466, 1335